Rising not falling? Differential compaction of shelf-edge trajectories and clinothem geometries

Daan Beelen[1,2], Christopher A-L. Jackson[1], Stefano Patruno[3], David M. Hodgson[4], João P. Trabucho Alexandre[2]

[1]Basins Research Group (BRG), Department of Earth Sciences and Engineering, Imperial College, London SW7 2AZ, c.jackson@imperial.ac.uk

[2] Department of Earth Sciences, Universiteit Utrecht, P.O. Box 80115 3508 TC Utrecht, the Netherlands, beelen4@hotmail.com, j.trabucho@uu.nl

[3] PGS, 4 The Heights, Brooklands, Weybridge, Surrey, KT13 0NY, United Kingdom, Stefano.Patruno@pgs.com

[4] School of Earth and Environment, University of Leeds, Leeds LS2 9JT, d.hodgson@leeds.ac.uk

ABSTRACT

Clinothems document the progradation of sedimentary strata. Their geometries allow us to define shelf-edge trajectories, which are widely used to infer variations in relative sea-level, spatial and temporal partitioning of depositional environments, and the timing of sediment delivery to the slope and basin-floor. Here, we present a novel perspective on trajectory reconstruction of buried successions, applying a decompaction technique that explicitly accounts for down-dip lithology variations within clinothems. We show that preferential compaction of fine-grained foresets and bottomsets results in a basinward rotation of trajectories and a distortion of primary clinothem geometries. In some cases, shelf-edge trajectories change from rising to apparently falling after burial, potentially leading to erroneous interpretations of original basin-margin physiography, relative sea level fluctuations, and incorrect predictions for the timing and volume of sediment transfer to deep water.

INTRODUCTION

A shelf-edge trajectory is the record of the shelf-to-slope rollover position through time in a basin-margin clinothem succession. Theoretically, trajectories are proportional to the ratio of sediment aggradation to progradation, and they can therefore be used to infer changes in the interplay between sediment supply and relative sea-level changes, and to predict the timing and volume of sediment transfer from continents to the oceans (Haq et al., 1987; Helland-Hansen and Martinsen, 1996; Helland-Hansen and Hampson, 2009; Henriksen et al., 2011). Rising trajectories coincide with significant topset aggradation and are associated with the deposition of fluvial channel deposits or lagoonal depositional systems (Bullimore et al., 2005). In contrast, flat or falling trajectories signal subaerial exposure of the continental shelf, fluvial incision of the shelf-slope rollover, and transfer of coarse sediment to the slope and basin-floor (Helland-Hansen and Hampson, 2009; Dixon et al., 2012).

Trajectory analysis can be undertaken on seismic reflection data (e.g. Anell and Midtkandal, 2015), well-log correlation panels (e.g. Carvajal and Steel, 2012; Patruno et al., 2015a), or outcrops (Steel and Olsen, 2002; Jones et al., 2015). In all cases, the studied successions are, or have been, deeply buried, and their clinothem geometries and associated trajectories have been distorted by loading and sediment compaction. To account for this, for instance when estimating paleo-water-depth by measuring clinothem heights (e.g. Plint et al., 2009; Patruno et al., 2015b), previous studies have backstripped and decompacted the overburden overlying a succession of clinothems (herein called “non-sequential decompaction”, e.g., Plint et al., 2009; Allen and Allen, 2013; Patruno et al., 2015a). In some instances, this simple method is followed by the decompaction of each successive clinothem, from youngest to oldest (herein called “sequential decompaction”; Steckler et al., 1999, Klausen and Helland-Hansen, 2018). However, even in these cases, dip-oriented lithological heterogeneity, which is common in almost all clinothem-bearing successions, are not accounted for despite likely being significant. For example, porosity-depth curves for topset, foreset, and bottomset deposits identified in well-log data in the Washakie Basin, USA (Carvajal and Steel, 2012), indicate that clay-rich foresets and bottomsets compact twice as much as sandy topsets in the same clinothem when subjected to three kilometers of burial (Sclater and Christie, 1980; supplementary information 1). This is despite that fact that the bottomsets in this particular succession are unusually sandy (Carvajal and Steel, 2012). Motivated by this limited understanding of how lithological variability impacts trajectory analysis and derived interpretations, our objectives are to: i) present a novel perspective to sequential decompaction that accounts explicitly for lithological variations within clinothems; ii) apply this method to a broad suite of datasets, including seismic reflection (Taranaki Basin, New Zealand), well-log (Washakie Basin, USA), and outcrop datasets (van Keulenfjorden, Svalbard, Norway) to reconstruct pre-burial clinothem trajectories and geometries; iii), quantify the effects of differences in the lithology fractions during different stages of clinothem burial; and iv) discuss implications of this approach on shelf-edge trajectory and clinothem geometry analysis.

METHODS

In this study, we consider siliciclastic clinothems consisting of sand- and claystone (often referred to as” mudstone” or “shale”). The mix of these two rock types is captured by the “Vshale” value, wherein 0 represents pure sand and 1 represents pure clay. This is a widely used yet somewhat simplistic approach as different depositional fabrics of clay mineralogies and silt grain types, such as flocs, result in a wide range of sorting arrangements, initial water content, and compaction behaviors (Potter et al., 2005). However, detailed mixed grain-size data are rarely reported from clinothems, and the key driver for differential compaction is the overall basinward fining from the topset to foreset/bottomset facies. This exists whether one chooses to implement simple or more complex grain size mixes. In our examples, Vshale values for topset, foreset, and bottomsets within individual clinothems are obtained from literature or, where available, derived directly from well-log or outcrop data (Johannessen et al., 2011; Carvajal and Steel, 2012). After determining Vshale values, a porosity/depth coefficient is calculated for each topset, foreset, and bottomset "compartment" using the empirically derived porosity/depth relations of Sclater and Christie (1980), although some have argued against the simplicity of these curves (Giles et al., 1998).

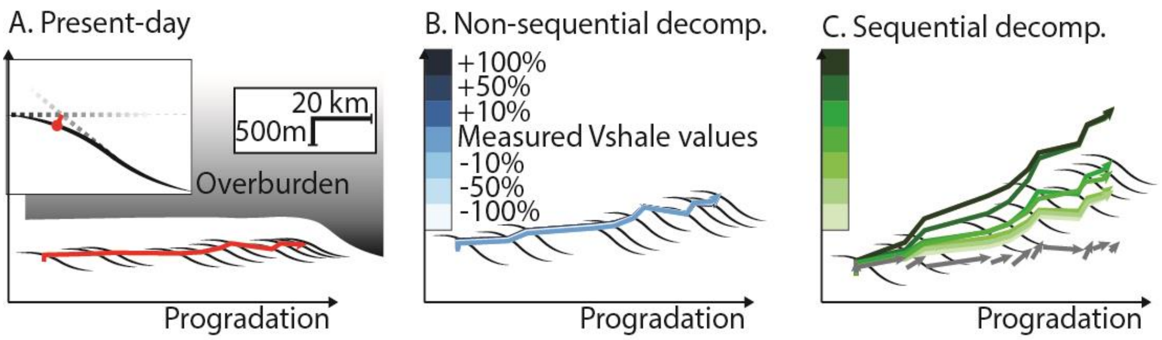

Figure 1. (A) Present shelf-edge trajectory (red) from Washakie Basin (Carvajal and Steel, 2012). Inset shows our geometric definition of the clinothem rollover point. (B) Non-sequentially decompacted trajectory (blue). (C) Sequentially decompacted trajectory (green), with unassembled trajectory increments shown as grey arrows (this step takes into account both the previous non-sequential decompaction and the successive application of the sequential decompaction of each single clinoform). Vshale values for topset, foreset, and bottomset are from Carvajal and Steel (2012). Colour gradients in B and C correspond to varying Vshale inputs. Note Low sensitivity in non-sequential decompaction and large sensitivity in sequential decompaction.

In our approach, we first backstrip, decompact, and unload all material overlying the target succession (‘non-sequential decompaction, e.g. Allen and Allen, 2013, Fig. 1B). This is followed by backstripping, decompaction, and unloading each individual clinothem in the succession, from youngest to oldest (‘sequential decompaction’, e.g. Steckler et al., 1999; Klausen and Helland-Hansen, 2018). This two-stage approach reconstructs each clinothem and its internal architecture back to its primary, unburied geometry. The trajectory within each reconstructed clinothem captures one increment of the complete trajectory that is reconstructed to its pre-burial state. The orientation and position of each reconstructed trajectory increment is recorded, and the complete trajectory is finally reconstructed by assembling all increments (Fig. 1C), which accounts for the effects of the continuous load-induced subsidence occurring during and after deposition of each consecutive clinothem. Vshale inputs for the non-sequential and sequential decompaction steps are the same. In both steps, a horizontal datum, one hundred meters below the base of the succession, was set as 0 burial. We define the location of the rollover point as the point of maximum curvature on the clinothem-bounding clinoform (inset Fig. 1A). Before decompaction, seismic datasets are depth-converted using check-shot data. We provide an extended outline of our methodology in the supplementary information (1). To examine how lithological uncertainty impacts our reconstructions of shelf-edge trajectories, we varied Vshale inputs by ±10, 50 and 100% (Fig. 1B and C). We do not account for the time-dependent component of isostasy. Considering that the timescale of shelf-edge clinothem deposition (ca. 1-5 mm/yr; Patruno et al., 2015b), is approximately equal to or slower than that of isostatic adjustments due to sediment load (ca.1-8 mm/yr; Ivins et al., 2007), subsidence is expected to approach isostatic equilibrium on the spatial and temporal scales considered in this study.

RESULTS

We first assess the accuracy of our workflow by comparing the reconstructed geometry of an ancient clinothem to that of an unburied, geometrically similar clinothem in the same formation (Giant Foresets Formation, Taranaki Basin, offshore New Zealand; Fig. 3). Similarities in the geometry, height, and slope gradient between the reconstructed (Fig. 3C) and unburied (Fig. 3D) clinothems suggest our method accurately reconstructs the overall geometry, internal architecture, and thus trajectory of the buried clinothem. The effects of applying our workflow on clinothem heights and slope gradients from Washakie Basin and van Keulenfjorden are shown in Figure 2.

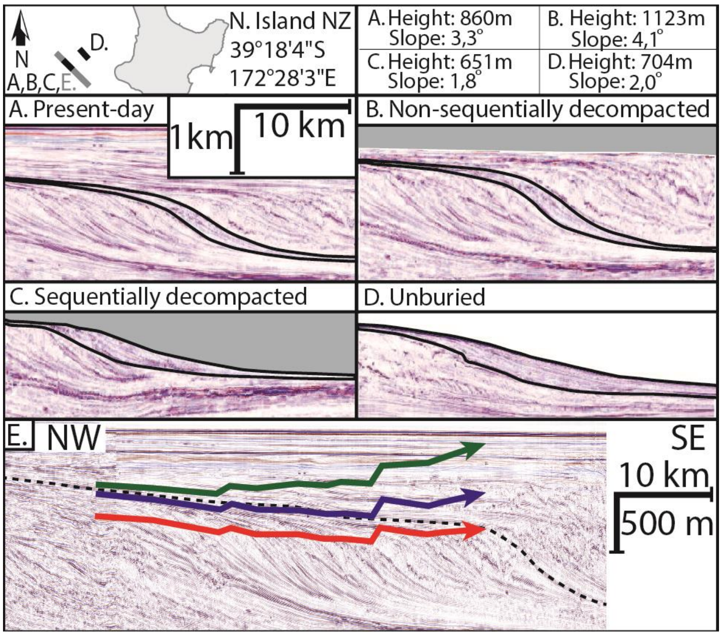

Figure 2. Buried (A) and unburied (D) clinothem geometries in the Taranaki Basin. (A) is located 60 km NE of (D), lying within same formation. Grey infill in (B) and (C) shows backstripped area. Numbers is top-right are clinothem height and slope gradient. Non-sequential decompaction with down-dip variation in lithology (i.e., from A to B) uniformly increases the height and slope gradient, whereas sequential decompaction, accounting for down-dip variation in lithology (i.e., from B to C),

decreases clinothem heights and slope gradients and results in a better similarity with the unburied geometry (D). Scale bar shown in (A) applies to B, C and D.

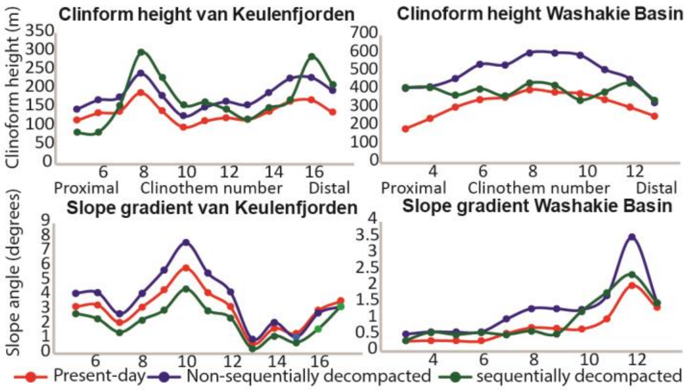

Figure 3. Graphs of present (red), non-sequentially (blue) and sequentially decompacted (green) clinoform heights and slope gradients from outcrop (van Keulenfjorden) and well-log (Washakie Basin) datasets. Clinothem heights are the vertical distance between the basin floor and the shelf/slope rollover. Slope gradients are the average gradient of the foreset. Not all clinothems in the successions are measured due to data limitations.

Clinothem geometries and their trajectory increments respond differently to the two steps of our decompaction methodology. Through step 1, the non-sequential decompaction, clinothem heights and slope gradients are overall uniformly increased (Fig. 2, from red lines to blue lines). Trajectory gradients also uniformly increase with respect to their present orientation (Fig. 3E). Although additional strata are backstripped during step 2, sequential decompaction, clinothem heights and slope gradients typically decrease rather than increase (Fig. 2, from blue lines to red lines). Overall, after non-sequential and then sequential decompaction, average trajectory gradients within each dataset are increased by 0.5° to 1.3° (Table 1).

Average trajectory gradient (degrees)	**Present**	**Step 1: non-sequential decompaction**	**Step 2: sequential decompaction**
Washakie Basin	0.3	0.7	1.3
van Keulenfjorden	1.1	1.8	2.4
Taranaki Basin	-0.1	0	0.4

Table 1. Average gradients across the entire length of the measured trajectory. Values are in degrees.

Changes in shelf-edge trajectory reflect variations in the ratio of aggradation to progradation (Helland-Hansen and Hampson, 2009). However, as we show here, the true shelf-edge trajectories change post-depositionally in response differential compaction and continuous subsidence due to sediment loading (Fig. 3E). For example, much of the presently falling trajectory (red arrow in Fig. 3E) in the Giant Foresets Formation was actually rising during progradation (green arrow in Fig. 3E). In this area, lithological data are available from nearby wells, though it should be noted that these data cannot constrain lithological variability within all clinothem compartments. Because of this, there is some uncertainty with regards to our Vshale inputs. However, the Washakie Basin sensitivity analysis tells us that a ±10% change in Vshale input results in an increase or decrease in trajectory orientation of 0.3°. Since the calculated trajectory reorientation are outside of this margin of error, it can be concluded that post-depositional trajectory reorientation has occurred here. Our interpretation that the observed falling trajectory in Taranaki Basin was actually rising during deposition is supported by the thick topset deposits, a stratigraphic architecture characterized by rising rather than falling trajectories (Helland-Hansen and Hampson, 2009). We applied our workflow to other datasets containing successive clinothems with falling trajectory (i.e. Columbus Basin, Trinidad, Chen et al. 2016; Karoo Basin, South Africa, Poyatos-Moré et al., 2016; see supplementary information 2). After decompaction, observed falling trajectory increments within both these datasets were reoriented to reveal rising trajectories.

DISCUSSION

We recognize two distinct stages in the burial and compaction of clinothem strata: i) “early” sequential compaction, which drives major differential (i.e. down-dip) compaction; and ii) “late” non-sequential compaction, which is associated with only minor differential compaction. During the sequential compaction stage, a basinward-fining clinothem is buried by a younger clinothem, and clay-rich foresets and bottomsets compact more than sand-rich topsets; this drives a steepening of the foreset strata, which is accompanied by vertical extension (i.e. an increase in height) of the clinothem (Fig. 4A). These observations contradict the results of a previous study by Deibert et al. (2003), who argue differential compaction decreases the height and slope gradient of the clinothem. The likely explanation for this disparity is that Deibert et al. (2003) do not account for down-dip changes in lithology within their decompacted clinothems. Vertical extension of the clinothem during the first (sequential decompaction) stage is, in most cases, greater than the overall compaction, causing a net increase in clinothem height and slope gradient (Fig 2, from green lines to blue lines).

The later non-sequential compaction stage starts when clinothems are buried below a simple, horizontally layered overburden, potentially consisting of shallow-marine shelf and coastal plain deposits. In this stage, the amount of differential compaction is much less than in the first, sequential decompaction stage. This is because, in most cases, during basin margin development, older, buried clinothems form sub-parallel belts of similar lithology due to the roughly horizontal alignment of topset, foreset, and bottomset compartments. This drives non-differential compaction, which decreases clinothem heights and slope gradients by evenly compressing the buried succession (Fig. 2, from blue lines to red lines, Fig. 4).

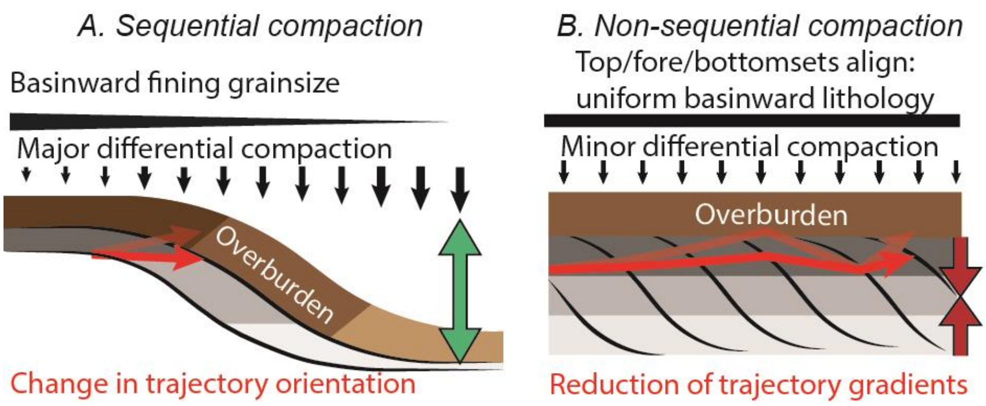

Figure 4. Impacts of (A) 'early', differential (i.e. sequential) compaction, and (B) 'late', non-differential (i.e. non-sequential) compaction on clinothem geometries and shelf-edge trajectories. Topset, foreset, and bottomset compartments indicated in gray shading. Note opposing effects with respect to clinothem height (decreases)and slope gradient (increases).

The two stages of compaction thus work in opposition with regards to their net effect on clinothem heights and slope gradients, meaning simple decompaction methodologies not including sequential decompaction, or that do not account for lithological heterogeneities within clinothems, need revision. In fact, previous application of previous methods may result in erroneous reconstructions of paleo basin depth (Plint et al., 2009; Patruno et al., 2015b), progradation rates and depositional fluxes (Patruno et al., 2015b), relative sea level fluctuations (Haq et al., 1987), and paleo slope gradients (Deibert et al., 2003).

There is also a shift in the response of the shelf-edge trajectory between the two stages of compaction. Sequential compaction causes a downward rotation of the trajectory due to differential compaction (Fig. 4A). Furthermore, in the case of significant progradation, mass is disproportionally applied to the area surrounding the inflection point, around the center of the foreset strata, causing additional basinward rotation of trajectories. This may also, in some cases, slightly depress strata underlying the clinothem foreset. Depression of strata underlying the inflection point can be seen in our reconstructed and unburied case studies from Taranaki Basin (Fig. 3C, D). The amount of reorientation depends on the rate and distribution of down-clinothem fining, and the amount of progradation during each increment. Non-sequential compaction then compresses the entire succession, and thereby roughly uniformly reduces trajectory gradients, with steeper positive gradients being reduced more than shallower ones (Fig. 4B; Patruno et al., 2015a). This difference in the response of the trajectory to the two phases of compaction can also be seen in the results of our sensitivity analysis, which indicates that the initial sequential compaction stage is especially sensitivity to lithological inputs (i.e. large divergence in results in Fig. 1C), whereas non-sequential compaction proceeds virtually irrespective of Vshale inputs (small divergence in results Fig. 1B), even though much more material is removed in the non-sequential decompaction step.

The strong reduction in differential compaction at the end of the sequential compaction stage is shelf-edge trajectory dependent. In the case of perfectly flat trajectories, non-sequential compaction will be completely non-differential. However, in cases of steeply rising shelf-edge trajectories, topset, foreset, and bottomset deposits will not be aligned perfectly within the clinothem successions. When this is the case, down-dip lithological changes will persist, though less prominently, as indicated by our sensitivity analyses that were performed on a trajectory with a rising orientation (Fig 1B). Future experiments that use more complicated ranges and distributions of lithologies are thereby likely to achieve even more accurate reconstructions of true shelf-edge trajectories and clinothem geometries. Another important observation is that topset surfaces, which are sometimes used to estimate paleohorizontal datums (e.g. Klausen and Helland-Hansen, 2018), can also be tilted basinward during the sequential compaction stage. Because of this, apparently falling shelf-edge trajectories with tilted topsets, such as the one from Taranaki Basin (Fig. 3E), are likely to have been reoriented due to differential compaction and loading. Correcting for topset surface tilt, like estimating topset aggradation, could therefore be used to estimate primary trajectory configurations without the need to apply decompaction.

CONCLUSIONS

By explicitly accounting for dip-oriented lithological heterogeneities within clinothem-bearing successions, we provide a novel refinement to the sequential decompaction workflow, using this to reconstruct primary shelf-edge trajectory orientations. We show that differential compaction and sediment loading cause major reorientations of the primary shelf-edge trajectory after burial. As a result, recorded trajectories that are observed in stratigraphy differ from true trajectories, and are not proportional to the rates of aggradation to progradation. These can lead to major differences, for example with originally rising trajectories being modified to be apparently falling. These results impact our ability to accurately reconstruct relative sea level fluctuations, infer depositional environments and depositional rates, and to infer the timing of basinward transfer of coarse-grained sediment. We also show that burial and geometric distortion of clinothems and their associated shelf-edge trajectories occurs in two distinct stages, whereby each stage has an approximately opposite net-effect with regards to the height and slope gradient of the clinothem. This emphasizes that simplistic, yet widely used decompaction methodologies that do not account for lithological heterogeneities, as well as the mass of individual clinothems in the succession, may need to be revised to ensure more accurate reconstructions of syn-depositional clinothem heights and slope gradients.

REFERENCES

Allen, P. A., and Allen, J. R., 2013, Basin analysis: Principles and application to petroleum play assessment, John Wiley & Sons.

Anell, I., and Midtkandal, I., 2015, The quantifiable clinothem–types, shapes and geometric relationships in the Plio-Pleistocene Giant Foresets Formation, Taranaki Basin, New Zealand: Basin Research, 29.S1: 277-297.

Bullimore, S., Henriksen, S., Liestøl, F. M., & Helland-Hansen, W., 2005, Clinoform stacking patterns, shelf-edge trajectories and facies associations in Tertiary coastal deltas, offshore Norway: Implications for the prediction of lithology in prograding systems: Norwegian Journal of Geology/Norsk Geologisk Forening, 85.

Carvajal, C., and Steel, R., 2012, Source-to-sink sediment volumes within a tectono-stratigraphic model for a Laramide shelf-to-deep-water basin: methods and results: Tectonics of Sedimentary Basins: Recent Advances, p. 131-151.

Chen, S., Steel, R.J. and Olariu, C., 2016. Upper-slope to shelf-edge delta architecture, Miocene Cruse Formation, Orinoco shelf margin, Trinidad. Journal of Sedimentary Research, 86(2), pp.87-106.

Deibert, J.E., Benda, T., Løseth, T., Schellpeper, M. and Steel, R.J., 2003. Eocene clinoform growth in front of a storm-wave-dominated shelf, Central Basin, Spitsbergen: no significant sand delivery to deepwater areas. *Journal of Sedimentary Research*, *73*(4), pp.546-558.

Dixon, J., Steel, R., and Olariu, C., 2012, Shelf-edge delta regime as a predictor of deep-water deposition: Journal of Sedimentary Research, v. 82, no. 9, p. 681-687.

Haq, B.U., Hardenbol, J.A.N. and Vail, P.R., 1987. Chronology of fluctuating sea levels since the Triassic. *Science*, *235*(4793), pp.1156-1167.

Hampton, M. A., Lee, H. J., and Locat, J., 1996, Submarine landslides: Reviews of geophysics, v. 34, no. 1, p. 33-59.

Helland-Hansen, W., and Martinsen, O. J., 1996, Shoreline trajectories and sequences: description of variable depositional-dip scenarios: Journal of Sedimentary Research, v. 66, no. 4.

Helland-Hansen, W., and Hampson, G., 2009, Trajectory analysis: concepts and applications: Basin Research, v. 21, no. 5, p. 454-483.

Henriksen, S., Helland-Hansen, W., and Bullimore, S., 2011, Relationships between shelf-edge trajectories and sediment dispersal along depositional dip and strike: a different approach to sequence stratigraphy: Basin Research, v. 23, no. 1, p. 3-21.

Giles, M.R., Indrelid, S.L. and James, D.M.D., 1998. Compaction—the great unknown in basin modelling. Geological Society, London, Special Publications, 141(1), pp.15-43.

Ivins, E.R., Dokka, R.K. and Blom, R.G., 2007. Post-glacial sediment load and subsidence in coastal Louisiana: Geophysical Research Letters, 34(16).

Johannessen, E. P., Henningsen, T., Bakke, N. E., Johansen, T. A., Ruud, B. O., Riste, P., Elvebakk, H., Jochmann, M., Elvebakk, G., and Woldengen, M. S., 2011, Palaeogene clinothem succession on Svalbard expressed in outcrops, seismic data, logs and cores: First Break, v. 29, no. 2, p. 35-44.

Jones, G. E., Hodgson, D. M., and Flint, S. S., 2015, Lateral variability in clinothem trajectory, process regime, and sediment dispersal patterns beyond the shelf-edge rollover in exhumed basin margin-scale clinothems: Basin Research, v. 27, no. 6, p. 657-680.

Klausen, T.G. and Helland-Hansen, W., 2018. Methods For Restoring and Describing Ancient Clinoform Surfaces. Journal of Sedimentary Research, 88(2), pp.241-259.

Patruno, S., Hampson, G. J., Jackson, C. A. L., and Whipp, P. S., 2015a, Quantitative progradation dynamics and stratigraphic architecture of ancient shallow-marine clinothem sets: a new method and its application to the Upper Jurassic Sognefjord Formation, Troll Field, offshore Norway: Basin Research, v. 27, no. 4, p. 412-452.

Patruno, S., Hampson, G. J., and Jackson, C. A., 2015b, Quantitative characterisation of deltaic and subaqueous clinothems: Earth-Science Reviews, v. 142, p. 79-119.

Plint, A. G., Tyagi, A., Hay, M. J., Varban, B. L., Zhang, H., and Roca, X., 2009, Clinothems, paleobathymetry, and mud dispersal across the Western Canada Cretaceous foreland basin:

evidence from the Cenomanian Dunvegan Formation and contiguous strata: Journal of Sedimentary Research, v. 79, no. 3, p. 144-161.

Potter, P. E., Maynard, J. B., and Depetris, P. J., 2005, Mud and mudstones: Introduction and overview, Springer Science & Business Media.

Poyatos-Moré, M., Jones, G.D., Brunt, R.L., Hodgson, D.M., Wild, R.J. and Flint, S.S., 2016. Mud-dominated basin-margin progradation: processes and implications. Journal of Sedimentary Research, 86(8), pp.863-878.

Sclater, J. G., and Christie, P., 1980, Continental stretching; an explanation of the post-Mid-Cretaceous subsidence of the central North Sea basin: Journal of Geophysical Research, v. 85, no. B7, p. 3711-3739.

Steckler, M. S., Mountain, G. S., Miller, K. G., and Christie-Blick, N., 1999, Reconstruction of Tertiary progradation and clinothem development on the New Jersey passive margin by 2-D backstripping: Marine Geology, v. 154, no. 1, p. 399-420.

Steel, R., and Olsen, T., Clinothems, clinothem trajectories and deepwater sands, *in* Proceedings Sequence-stratigraphic models for exploration and production: Evolving methodology, emerging models and application histories: Gulf Coast Section SEPM 22nd Research Conference, Houston, Texas2002, p. 367-381.

Supplementary information 1

1) A dip-section image of a clinoform bearing succession is selected from literature. Example: Washakie Basin obtained from (Carvajal and Steel, 2012).

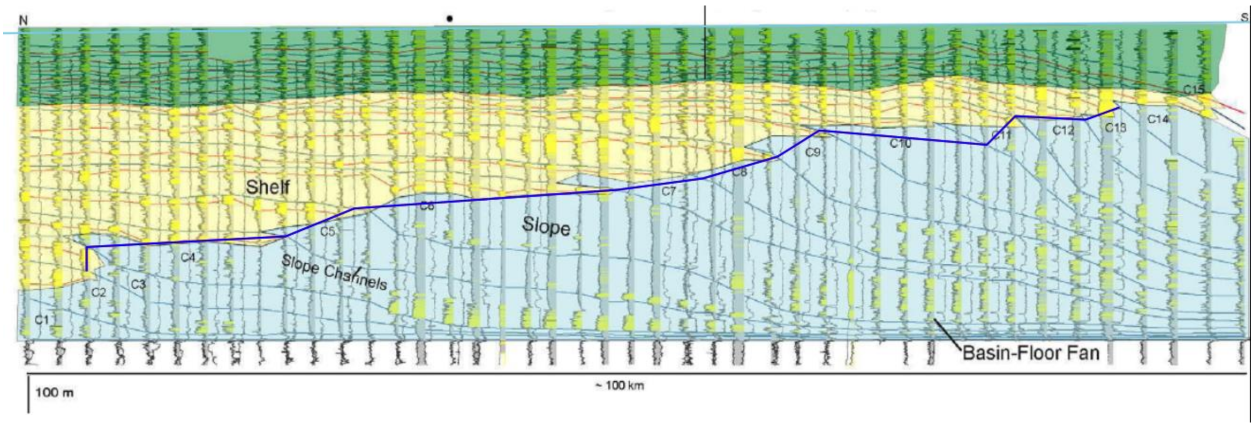

2) The image is imported into Midland Valley Move software and scaled appropriately. The basinal overburden is added (in this case 3300 m).

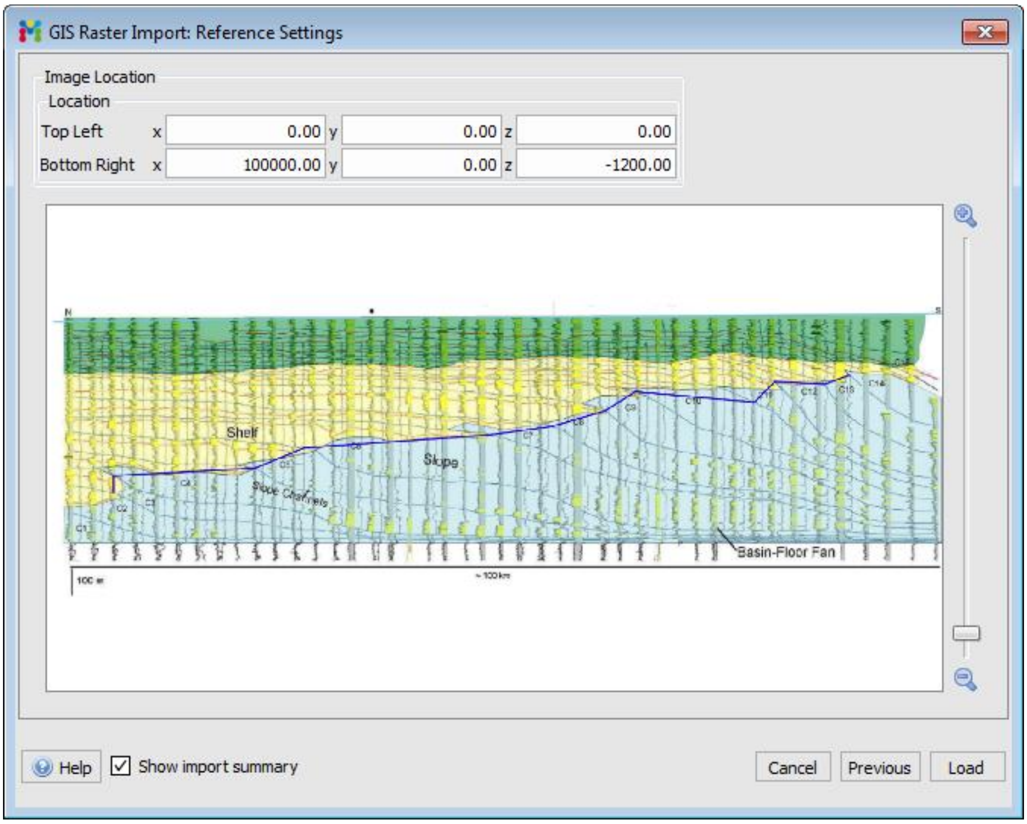

3) Horizons are constructed to delineate clinothems. The overburden is constructed (blue).

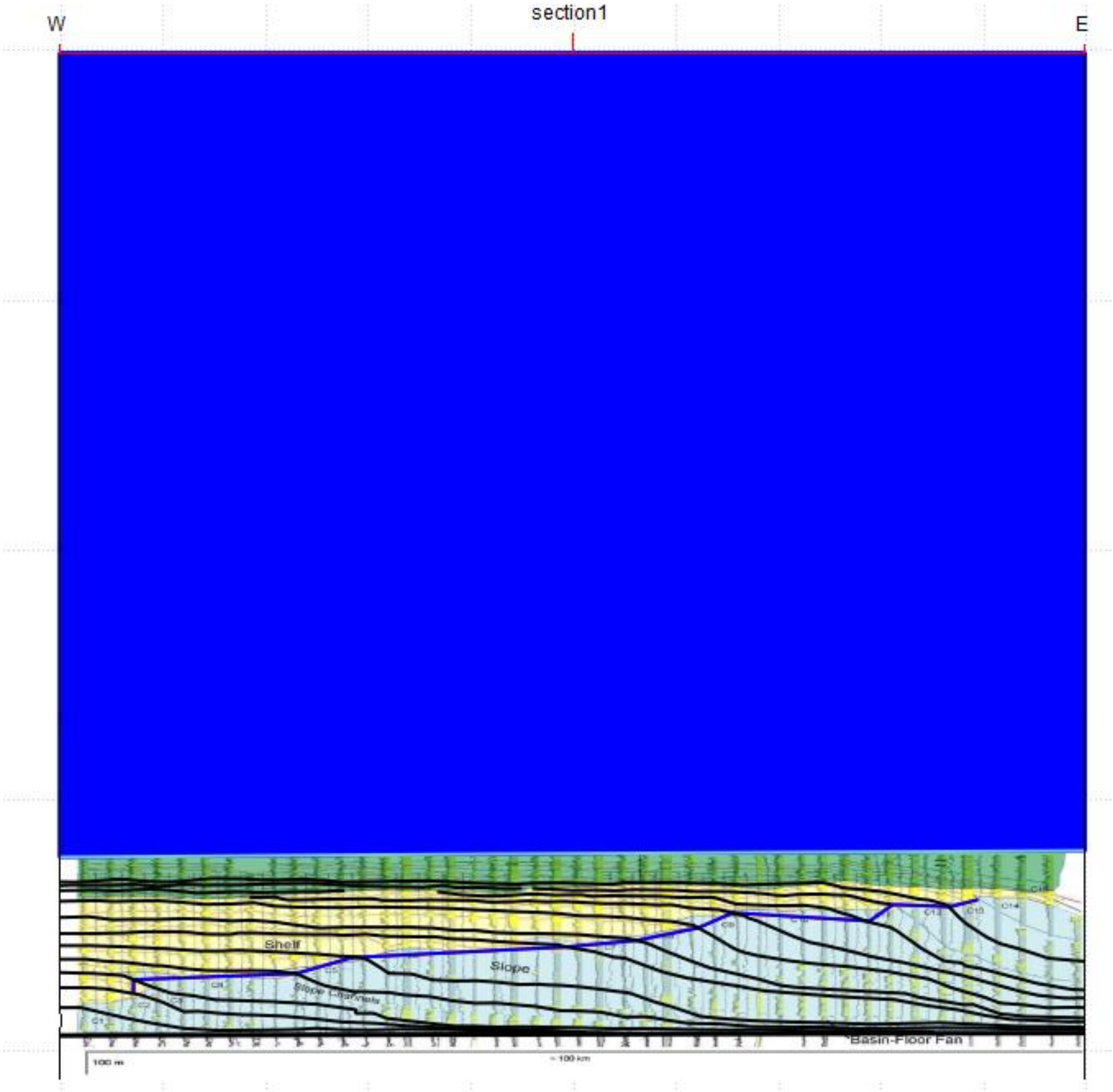

4. A polygon is constructed for each topset (green), foreset (yellow) and bottomset (red) compartment in the succession.

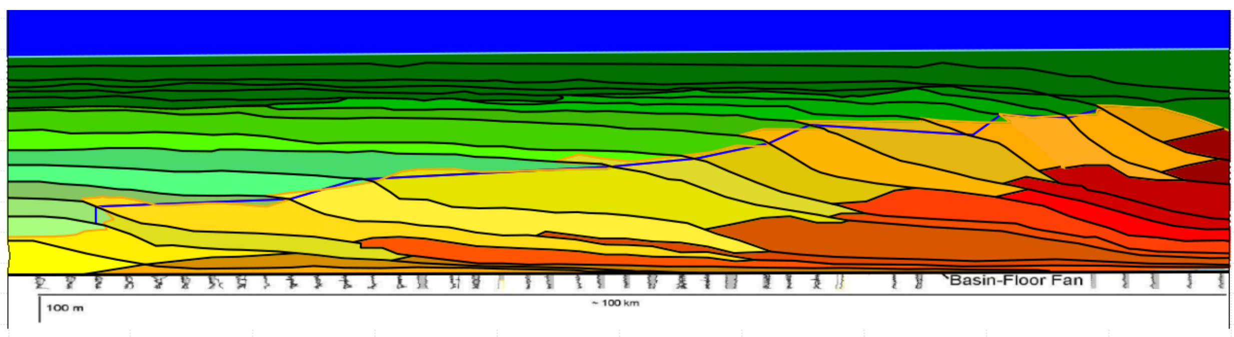

5a. Vshale ratios are obtained from literature, in this case (Carvajal and Steel 2012).

Table 7.1. Clinothem (C) volumes for sandstone (Vss), shale (Vsh), and coal (Vc). TOP = topset, SL = slope, BF = basin floor, and TOT = total (compartment areas may overlap, for instance at the shelf edge, see Fig. 7.4)

		A km^2	Vss km^3	Vss %	Vsh km^3	Vsh %	Vc km^3	TOT km^3	TOT %	Ss/Sh ratio	Ss Mass × 10^9 ton	Sh Mass × 10^9 ton	TOT Mass × 10^9 ton
1	TOP	0	0.0	0.0	0.0	0.0	0.0	0.0	0		0.0	0.0	0.0
	SL	71	1.3	23.7	4.8	5.0		6.1	6	0.28	2.2	11.0	13.3
	BF	8708	4.3	76.3	90.6	95.0		94.8	94	0.05	7.1	210.1	217.2
	TOT		5.6		95.4		0.0	100.9		0.06	9.4	221.1	230.5
2	TOP	159	2.2	8.9	4.4	3.8	0.0	6.7	5	0.50	3.7	10.3	14.0
	SL	403	12.1	48.4	27.5	23.5		39.7	28	0.44	20.4	63.9	84.2
	BF	8217	10.7	42.7	85.1	72.7		95.8	67	0.13	17.9	197.3	215.2
	TOT		25.0	100.0	117.1	100.0	0.0	142.1		0.21	42.1	271.4	313.5
3	TOP	234	5.6	33.2	5.1	3.4	0.0	10.8	6	1.10	9.4	11.9	21.3
	SL	1312	11.2	66.1	73.3	48.8		84.5	51	0.15	18.8	170.1	188.9
	BF	7308	0.1	0.7	71.8	47.8		71.9	43	0.00	0.2	166.4	166.6
	TOT		16.9	100.0	150.2	100.0	0.0	167.2		0.11	28.4	348.4	376.8
4	TOP	1688	24.8	24.7	33.2	9.6	0.4	58.4	13	0.75	41.6	77.0	118.6
	SL	1656	26.3	26.3	121.8	35.2		148.1	33	0.22	44.3	282.4	326.6
	BF	6888	49.1	49.0	191.2	55.2		240.3	54	0.26	82.5	443.4	525.9
	TOT		100.2	100.0	346.2	100.0	0.4	446.8		0.29	168.3	802.8	971.1
5	TOP	1916	39.4	54.9	75.4	20.5	0.1	114.8	26	0.52	66.2	174.7	240.9
	SL	1960	12.6	17.6	144.0	39.3		156.6	36	0.09	21.2	334.0	355.2
	BF	5131	19.7	27.5	147.4	40.2		167.2	38	0.13	33.2	341.8	375.0
	TOT		71.7	100.0	366.8	100.0	0.1	438.6		0.20	120.5	850.6	971.1
6	TOP	3008	68.0	43.7	111.7	23.4	0.2	180.0	28	0.61	114.3	259.0	373.3
	SL	2804	21.7	13.9	203.5	42.6		225.2	36	0.11	36.5	471.9	508.4
	BF	4059	65.9	42.3	163.0	34.1		228.9	36	0.40	110.7	378.0	488.7
	TOT		155.6	100.0	478.2	100.0	0.2	634.1		0.33	261.4	1108.9	1370.4
7	TOP	3394	55.6	65.6	98.4	37.9	0.3	154.3	45	0.57	93.5	228.2	321.7
	SL	2125	10.4	12.3	80.8	31.1		91.3	26	0.13	17.5	187.4	204.9
	BF	3645	18.8	22.2	80.5	31.0		99.3	29	0.23	31.6	186.8	218.3
	TOT		84.8	100.0	259.8	100.0	0.3	344.9		0.33	142.5	602.4	744.9

5b. In case Vshale numbers cannot be obtained from literature, they are derived from images of published well logs using image compartmentalization and color segmentation tools (magic wand tool in Adobe Photoshop). Number of pixels is counted in order to determine the relative contribution of sand vs shale. Example: Taranaki Basin, log published in (M. Salazar et. al 2015).

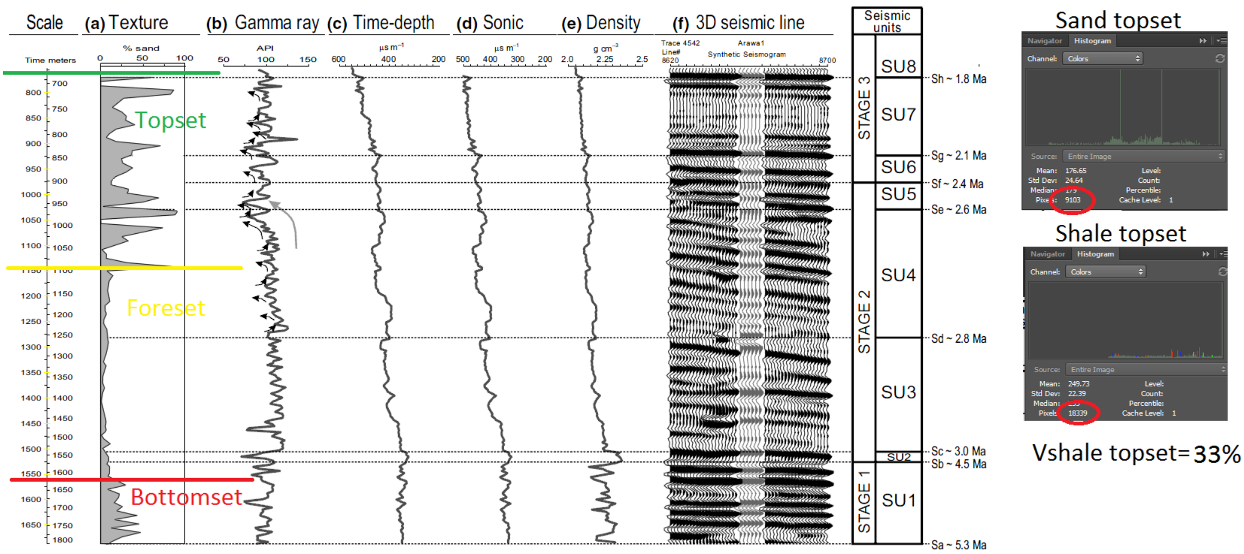

6. A Vshale number is designated for each compartment. Afterwards, compartmental compaction curves are constructed using empirically derived compaction relations from Sclater Christie, 1980: $f = f_0(e^{-cy})$ Where f is present day porosity at depth, f_0 is the porosity at the surface, c is the porosity-depth coefficient (km^{-1}) and y is depth. The percentage of sandstone and shale is converted into surface porosities and depth coefficient values using the average decompaction values for North Sea sediments by Sclater and Christie (1980). The initial sandstone and shale percentages are multiplied by the appropriate surface porosity and compaction coefficient values from Sclater and Christie (1980). This resultant value (c) is used as the input value for the parameters in the decompaction algorithm.

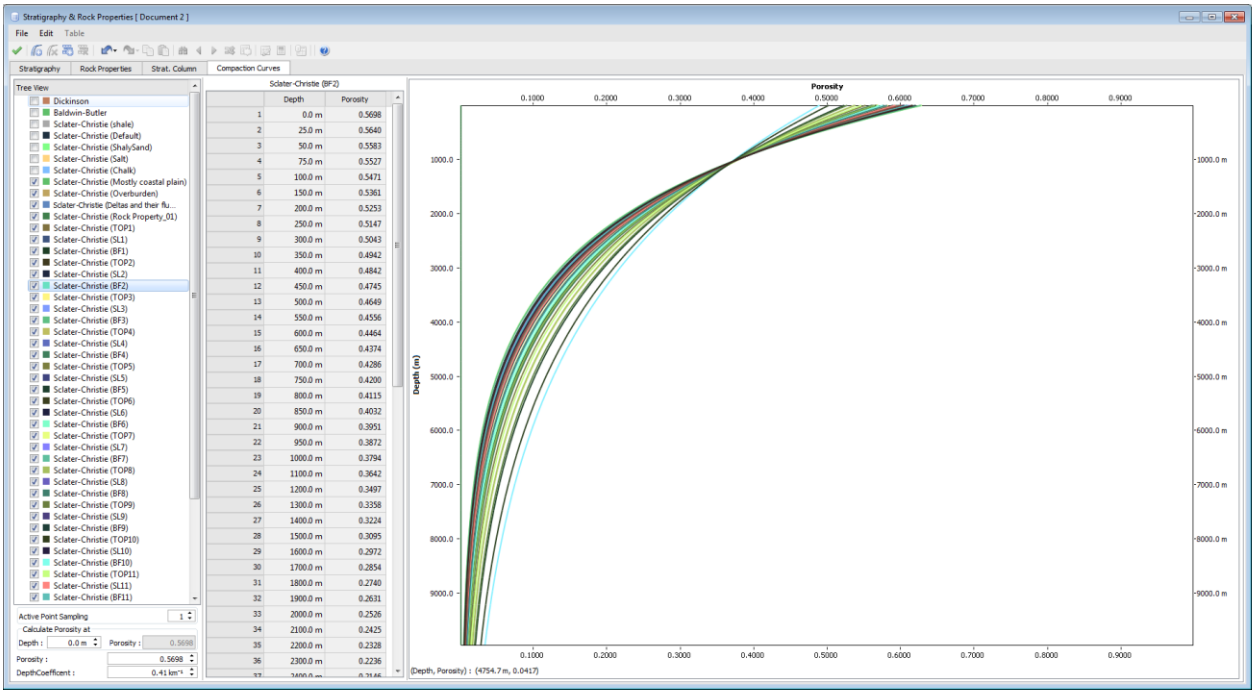

7. Non-sequential compaction of the succession overburden is applied. During each decompaction experiment, 100-500 equally spaced, one-dimensional vertical columns along the succession are constructed. Afterwards, the overburden is backstripped. Volume increase is calculated by upscaling the length of the columns based on reducing porosity loss in accordance with the porosity/depth relation. The following animation shows non-sequential decompaction of the Washakie Basin dataset. The overburden was decompacted in three phases in order to show intermediate stages of non-sequential compaction. (Double click to open animation).

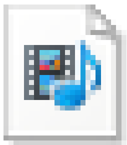

Non-sequential decompaction.mp4

8. Afterwards, each clinothem is decompacted successively starting from the youngest, most distal to the oldest, most proximal clinothem. The following animation shows sequential decompaction of the Washakie Basin dataset. In this example, polygons are visualized. Section is from (Koo et al. 2016). (Double click to open animation).

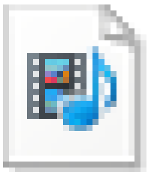

Sequential decompaction.mp4

9. After each phase of decompaction, the position and orientation of every reconstructed trajectory increment, one for every clinothem, is recorded.

10. Trajectory increments are assembled end-to-end. This corrects for the isostatic readjustments that occur after each step. These Isostatic readjustments due to unloading are calculated through applying an Airy isostasy (Airy, 1856). The following relation is applied:

$$Z = \frac{S - (H1 - H2)\rho_c - \rho_w}{\rho_m - \rho_w}$$

Where *Z* is the amount of subsidence (relative to a basement datum), *S* is the thickness of the unloaded sediment. *H1* is crustal thickness before sediment load, *H2* crustal thickness after sediment load. ρ_c ρ_m and ρ_w are the densities of crust, mantle and water respectively. As indicated by these models.

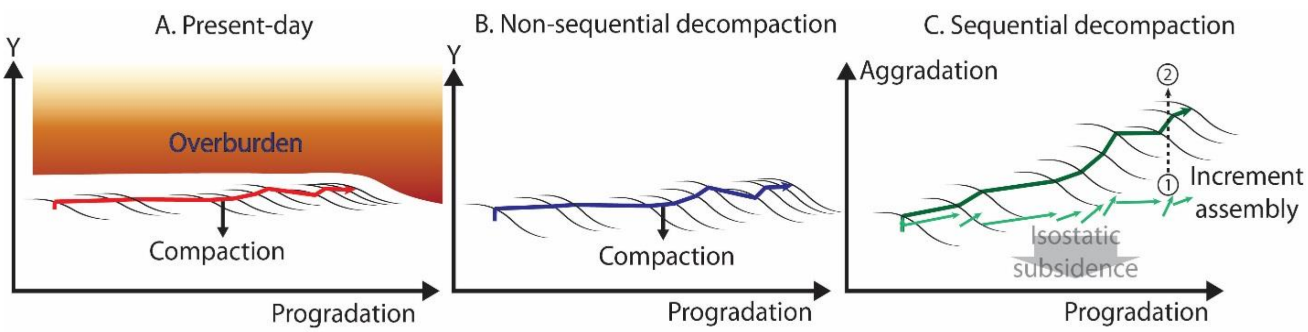

11. The present-day trajectory is compared to the non-sequentially and sequentially decompacted trajectories. Example: van Keulenfjorden (Steel and Olsen 2002).

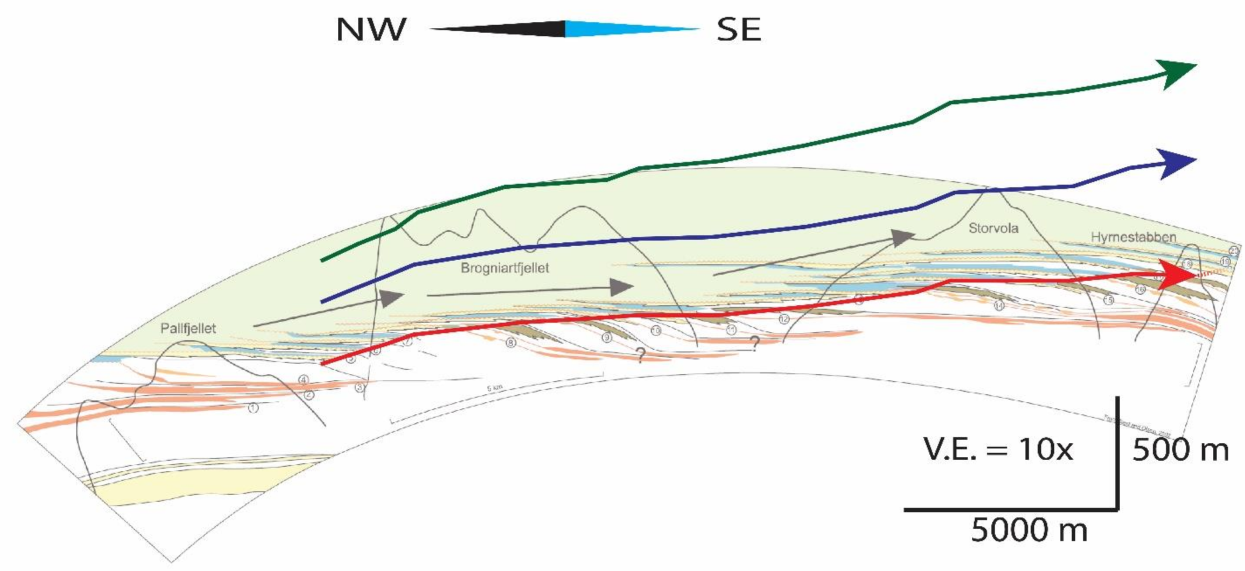

Supplementary information 2

Karoo, Ecca Group

Removal of the 6300-meter overburden displaces the trajectory significantly. Moreover, Trajectory gradients are increased by decompaction. The main observation is that the slightly falling -0.30° distal end of the Baviaans-North profile (wfC 5,6,7,8) is adjusted to a 0.05° flat trajectory (figure 11). Sequential decompaction indicates no significant alteration of syn-depositional clinoform geometries. A third observation is a loss of curvature and general flattening in the geometry of the unit F formation; the oldest formation in the Ecca-group clinoformal succession (Jones et al., 2015).

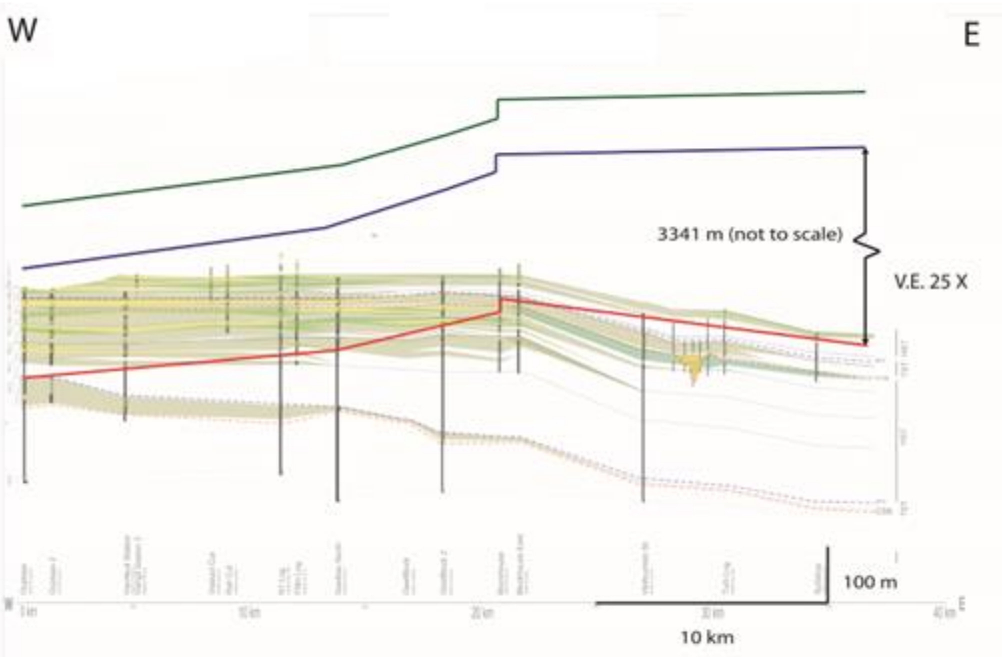

Columbus Basin

The Columbus Basin profile illustrates a stepwise aggradation dominated/progradation dominated shelf-edge trajectory. Because there is a limited overburden, there is only a small change in the trajectory following non-sequential decompaction. Sequential decompaction causes an overall increase in gradient with a downward to upward trajectory adjustment in the fourth sequence of the succession (TP44). Extremely steep sequentially decompacted trajectory intervals indicate extensive aggradation, this is further exaggerated following decompaction. Note that the profile is not depth-converted, this means that the absolute values for trajectory angles cannot he be determined, relative alterations in gradient and orientation after decompaction can however be recognised.

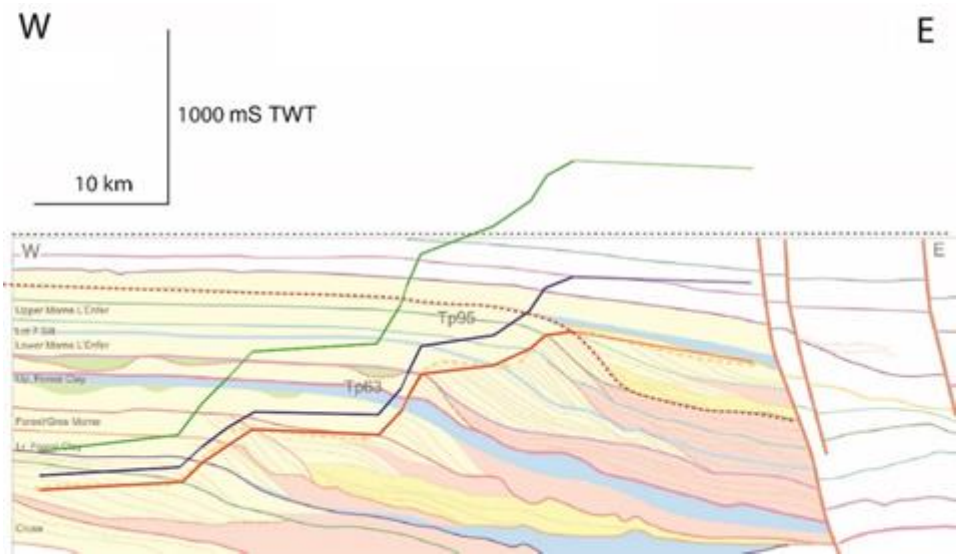

Chen, S., Steel, R.J. and Olariu, C., 2016. Upper-slope to shelf-edge delta architecture, Miocene Cruse Formation, Orinoco shelf margin, Trinidad. Journal of Sedimentary Research, 86(2), pp.87-106.

JONES, G. E., HODGSON, D. M. & FLINT, S. S. 2015. Lateral variability in clinoform trajectory, process regime, and sediment dispersal patterns beyond the shelf-edge rollover in exhumed basin margin-scale clinothems. *Basin Research,* 27**,** 657-680.

Poyatos-Moré, M., Jones, G.D., Brunt, R.L., Hodgson, D.M., Wild, R.J. and Flint, S.S., 2016. Mud-dominated basin-margin progradation: processes and implications. Journal of Sedimentary Research, 86(8), pp.863-878.